axis rotation brought about by the application of a magnetic field during irradiation, suggests that for the pure Fe and pure Ni films there is a realignment of defects and for the alloy films, there is a directional short-range ordering of Fe–Fe pairs of atoms or a combination of these two processes.

ACKNOWLEDGMENTS

The authors wish to thank the following people for their help: Dr. J. S. Mendousse for discussing an application of elasticity theory; C. M. Williams and T. J. McCartney for evaporating the films; Mrs. Janet P. Mason for programming the solution of a cubic equation; E. J. Brooks and O. R. Gates for the x-ray fluorescent and wet chemical analysis of the film composition; Carl Vold for determining the orientation of the single-crystal quartz substrate; C. M. Herbert for cutting the substrates; and Dr. P. R. Malmberg and W. H. Jones for helping with the Van de Graaff irradiations.

JOURNAL OF APPLIED PHYSICS VOLUME 38, NUMBER 10 SEPTEMBER 1967

Mobility of Edge Dislocations in the Basal-Slip System of Zinc*

D. P. Pope, T. Vreeland, Jr., and D. S. Wood

W. M. Keck Laboratories, California Institute of Technology, Pasadena, California

(Received 28 April 1967)

This paper presents the results of measurements of the velocities of $\langle 1\bar{2}10\rangle$ (0001) edge dislocations in zinc as a function of applied shear stress. All tests were conducted at room temperature on 99.999% pure zinc monocrystals. Dislocations were revealed by means of the Berg–Barrett x-ray technique. Stress pulses of microsecond duration were applied to the test specimens by means of a torsion testing machine. Applied resolved shear stresses ranged from 0 to 17.2×10^6 dyn/cm^2 and measured dislocation velocities ranged from 40–700 cm/sec.

The results of this study indicate that the velocity of edge dislocations in the basal slip system of zinc is linearly proportional to the applied resolved shear stress. These results are analyzed in terms of the phonon-drag theory. Agreement between this theory and the results reported here is quite good.

INTRODUCTION

There has been considerable dislocation mobility data gathered on various materials in recent years. The materials on which these measurements have been made are lithium fluoride,[1] silicon–iron,[2] sodium chloride,[3] tungsten,[4] various semiconductor crystals,[5–7] zinc,[8] and copper.[9] The data on zinc[8] were taken over quite a restricted stress and velocity range due to testing equipment limitations. It should be noted that all the crystals mentioned above except zinc and copper have either covalent or ionic bonding, or have a bcc crystal structure. Dislocations in these materials move at velocities far less than 1 cm/sec at the macroscopic yield point. However, in copper and zinc, an fcc metal and a hcp metal, respectively, the dislocations move at velocities well over 1 cm/sec at the yield point. The paucity of mobility data on fcc and hcp metals, materials in which the dislocations move rapidly at low stresses, is not due to a lack of interest in these materials, but rather due to the lack of suitable experimental techniques for handling and testing these very fragile crystals. It is the scarcity of mobility data on these materials that prompted the work reported here.

The studies made by Adams[8] exhibited two important facts about mobility measurements of basal dislocations in zinc; basal dislocations move rapidly at low stresses, and the velocities obtained from indirect strain rate measurements were very different from those obtained from direct measurements. Thus, it was decided to embark on an experimental program to make direct measurements of basal dislocation velocities as a function of applied shear stress in high-purity (99.999%) low-dislocation-density zinc single crystals.

A series of preliminary tests showed that the double-etch technique, the technique successfully used in copper,[9] was not suitable for these experiments on zinc. First, the basal dislocation density could not be reduced to a level where it was possible to follow the displacement of an individual dislocation, and second, sources of large numbers of mobile dislocations could not be produced at selected, isolated sites in zinc. If these sources could be produced, perhaps the motions of large groups of dislocations could be observed even with a high background density.

It was found that by using the Berg–Barrett x-ray

* This work was supported by the U.S. Atomic Energy Commission.

[1] W. G. Johnston and J. J. Gilman, J. Appl. Phys. **30**, 129 (1959).

[2] D. F. Stein and J. R. Low, Jr., J. Appl. Phys. **31**, 362 (1960).

[3] E. Yu. Gutmanas, E. M. Nadgornyi, and A. V. Stepanov, Soviet Phys.—Solid State **5**, 743 (1963).

[4] H. W. Schadler, Acta Met. **12**, 861 (1964).

[5] A. R. Chaudhuri, J. R. Patel, and L. G. Rubin, J. Appl. Phys. **33**, 2736 (1962).

[6] M. N. Kabler, Phys. Rev. **131**, 54 (1963).

[7] T. Suzuki and H. Kojima, Acta Met. **14**, 913 (1966).

[8] K. H. Adams, T. Vreeland, Jr., and D. S. Wood, Mater. Eng. Sci. **2**, 37(1967).

[9] W. F. Greenman, Ph. D. thesis, California Institute of Technology, Pasadena, Calif. (1966).

diffraction method for dislocation observations, both of the above-mentioned problems were avoided. Furthermore, the Berg–Barrett method yields an image of the dislocation line as opposed to the etch technique which shows only the intersections of dislocations with free surfaces. Also, the x-ray technique allows the determination of the Burgers vector of individual dislocations. Thus, the Berg–Barrett technique yields considerably more information about the dislocations being observed than does the etch technique.

All tests were conducted at room temperature on high-purity annealed zinc monocrystals machined into right circular cylinders. The longitudinal axes of the cylinders were parallel to the crystallographic c axis and the ends were parallel to the basal plane. Edge dislocations were produced on one end of each specimen by scratching the surface with an Al_2O_3 whisker loaded with 50 mg. The scratched surface of the specimen was glued to a loading fixture and a torsion pulse of about 50–100 μsec duration was applied to the specimen. The final dislocation configuration around the scratches was observed by means of the Berg–Barrett x-ray technique.

TEST-SPECIMEN PREPARATION

Single crystals were grown from 99.999% pure zinc obtained from Eagle-Picher Company, Miami, Oklahoma. The crystals were grown in graphite-coated Pyrex molds 3.5 cm in diameter and 25 cm long. The growth technique has been described by Stofel.[10] After the bulk crystal was removed from the Pyrex mold, the orientation of the basal plane was determined by cleaving a piece of the crystal in liquid nitrogen. Great care was taken to cool and heat the material no faster than 3°C/min to avoid plastic strains due to nonuniform thermal expansion. The bulk crystal was then acid-cut into rough cylinders with (0001) axes and having at least one cleaved basal plane end. The cleaved basal plane of the rough cylinder was then glued to a block of monel alloy R405 using Duco cement. Monel R405 alloy was used because its coefficient of thermal expansion closely matches that of zinc in the basal plane. The specimen was then placed in an acid lathe similar to that used in Ref. 10 and turned to 1.10-cm diam. Observation surfaces of test specimens were prepared either by cleaving or acid-lapping. The acid-lapped surfaces were prepared on a machine which is similar to the acid lathe. The specimens were then polished as described in Ref. 11. Finished specimens varied in length from 0.97–1.3 cm.

All specimen surfaces had to be very clean to prevent contamination of the testing surface during annealing. The specimens were annealed in pure hydrogen at 370°C for $\frac{1}{2}$ to 3 h. The hydrogen was purified by diffusion through a commercially available palladium purification unit. Specimens with an acid-lapped observation surface were ready for testing after this anneal. However, two separate annealing operations were required during the production of a specimen with a cleaved test surface, the first anneal making it easier to subsequently produce a smooth, step-free cleavage surface. Berg–Barrett photographs of annealed specimens showed only a few isolated basal dislocations inside the subgrains. The low dislocation density is typical of the material very near the observation surface and is not typical of the bulk material. This low dislocation density is due to the ease with which dislocations near the surface can climb and/or cross-glide out of the specimen during the anneal.

EXPERIMENTAL TECHNIQUES

Method for Producing Dislocations to be Studied

Edge dislocations were produced by scratching the basal plane observation surface of the test specimens. Three scratches, each made on a diameter along the $\langle 10\bar{1}0\rangle$ directions, were made on each specimen by an Al_2O_3 whisker fastened to an arm supported by a calibrated torsion wire. The force on the whisker was 50 mg. The scratches were made in segments approx 0.050 cm long with 0.008-cm gaps between each segment. Subsequent Berg–Barrett photographs showed the dislocations produced to be edge-oriented and lying in the basal plane with $\langle 11\bar{2}0\rangle$-type Burgers vectors. The orientation of the scratch on the basal plane relative to the crystal structure is shown in Fig. 1.

X-Ray Technique for Observing Dislocations

Dislocations in the basal plane were observed by means of the Berg–Barrett x-ray technique as used by Armstrong and Schultz[12] for photographing zinc. Characteristic Co radiation from a Machlett A-2 diffraction tube operating at 39 kV and 9 mA was used. The reflecting planes used were the $\{10\bar{1}3\}$. The images were recorded on Kodak high-resolution plates exposed for 6–8 h. An iron filter 0.0025 cm thick was placed between the specimen and film to prevent any fluorescence from reaching the plate. X-rays of the wavelength used are absorbed by zinc to the extent that only those dislocations are imaged which lie within a layer about 5μ below the observation surface.

The Burgers vector of a dislocation may be determined by making use of the fact that a dislocation produces an image on a photographic plate only when

$$\mathbf{b}\cdot\mathbf{n}\neq 0, \tag{1}$$

[10] E. J. Stofel, Ph.D. thesis, California Institute of Technology, Pasadena, Calif. (1962).

[11] R. C. Brandt, K. H. Adams, and T. Vreeland, Jr., J. Appl. Phys. **34**, 591 (1963).

[12] J. M. Schultz and R. W. Armstrong, Phil. Mag. **10**, 497 (1964).

where **b** is the dislocation Burgers vector and **n** is the normal to the reflecting plane.[13] Thus, a dislocation does not produce an image when its Burgers vector lies in the reflecting plane.

The Burgers vector of a given dislocation may be determined by finding two independent reflecting planes for which $\mathbf{b}\cdot\mathbf{n}=0$. The dislocation Burgers vector is then known to lie along the intersection of those two reflecting planes. The Burgers vectors of the dislocations produced by scratching were known to lie in the basal plane since the dislocations form no image in a (0004) reflection. The orientations of the Burgers vectors in the basal plane were found by determining which $\{10\bar{1}3\}$ reflection produced no contrast along the dislocation.

Loading System

A torsion impact machine developed for this work applies a single zero-mode torsional loading pulse of controlled duration to the specimen.[14] The machine generates a 2 μsec risetime wavefront. The wavefront travels through a 1.10-cm-diam Monel rod and into the 1.10-cm-diam zinc specimen, the observation surface of the specimen having been glued to the Monel rod. The wave after passing through the specimen reflects from a free surface and unloads the specimen. Calibrated semiconductor strain gauges were glued to the Monel rod 0.150 cm from the Monel–specimen interface to monitor the stress pulse on the surface at that point. The loading times were varied by gluing various lengths of 1.15-cm-diam titanium rods to the specimens. The diameter of the titanium was adjusted so that there was no reflection of the elastic wave at the titanium–specimen interface. The method for determining the proper diameter was discussed by Greenman.[9] The diameter of the zinc and Monel were made the same to avoid local perturbations in the stress state over the observation surface. This resulted in a partial reflection (approx 10%) of the stress wave at the interface. However the nearby strain gauges measured the surface stress at the interface, and that stress was read directly from the oscilloscope record.

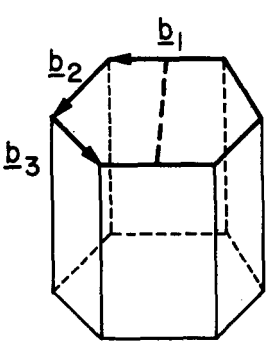

FIG. 1. Schematic diagram showing the relative orientations of a $\langle 10\bar{1}0\rangle$ scratch and the possible basal Burgers vectors in the unit cell. The scratch shown here produces edge dislocations of Burgers vector $\pm b_1$.

Gluing Technique for Fastening Specimens to Torsion Machine

Since the dislocation displacements were measured on the face of the specimen glued to the torsion machine, it was imperative that plastic strains were not introduced to that face by the gluing process or by differential thermal expansion. Thermal strains were avoided by gluing the observation surface of the specimen to Monel R405, an alloy whose coefficient of thermal expansion closely matches that of zinc in the basal plane.

The common glues that were tried were found to be unusable because they either produced large stresses in the specimen by shrinkage, solidified with voids, or produced bonds which were difficult to break. Phenyl salicilate (salol) was found to be a satisfactory glue if its large volume change upon solidification is compensated for in the following manner. The specimen is coated with a 0.01 cm$\pm$0.002-cm-thick void-free seed layer of salol by spraying the surface with a solution of 2 g salol in 25 ml of acetone from an artist's air brush. The monel is separately coated with molten salol and supercooled to room temperature. The two surfaces are then put together and the seed layer nucleates the bond simultaneously over the entire surface to be glued. The resulting bond is easily parted by soaking for about 5 min in acetone. The gluing operation produces dislocation displacements of less than 0.002 cm from fresh scratches.

Experimental Procedure

Berg–Barrett x-ray photographs were taken of annealed and scratched specimens prior to testing to determine the initial dislocation configuration around the scratches. However, the time required to take the photographs was sufficient for the dislocations around the scratches to become relatively immobile, presumably due to pinning by point defects. Consequently, specimens were stressed in the torsion-loading machine immediately after scratching without taking an initial Berg–Barrett photograph. The time between scratching and loading was typically about 1 h. Berg–Barrett photographs were taken of the specimens immediately after loading to determine the final dislocation configuration around the scratches. The method used for separating the dislocation displacements due to the scratching operation from the displacements due to the stress pulse is described in the next part of this paper.

Three specimens were tested, one having an acid-lapped observation surface and two having cleaved observation surfaces. The shear stress on the periphery of the specimens ranged from 9.7 to 17.2×10^6 dyn/cm^2. The combined length of the specimens and titanium

[13] J. B. Newkirk, AIME Trans. **215**, 483 (1959).
[14] D. P. Pope, T. Vreeland, Jr., and D. S. Wood, Rev. Sci. Instr. **35**, 1351 (1964).

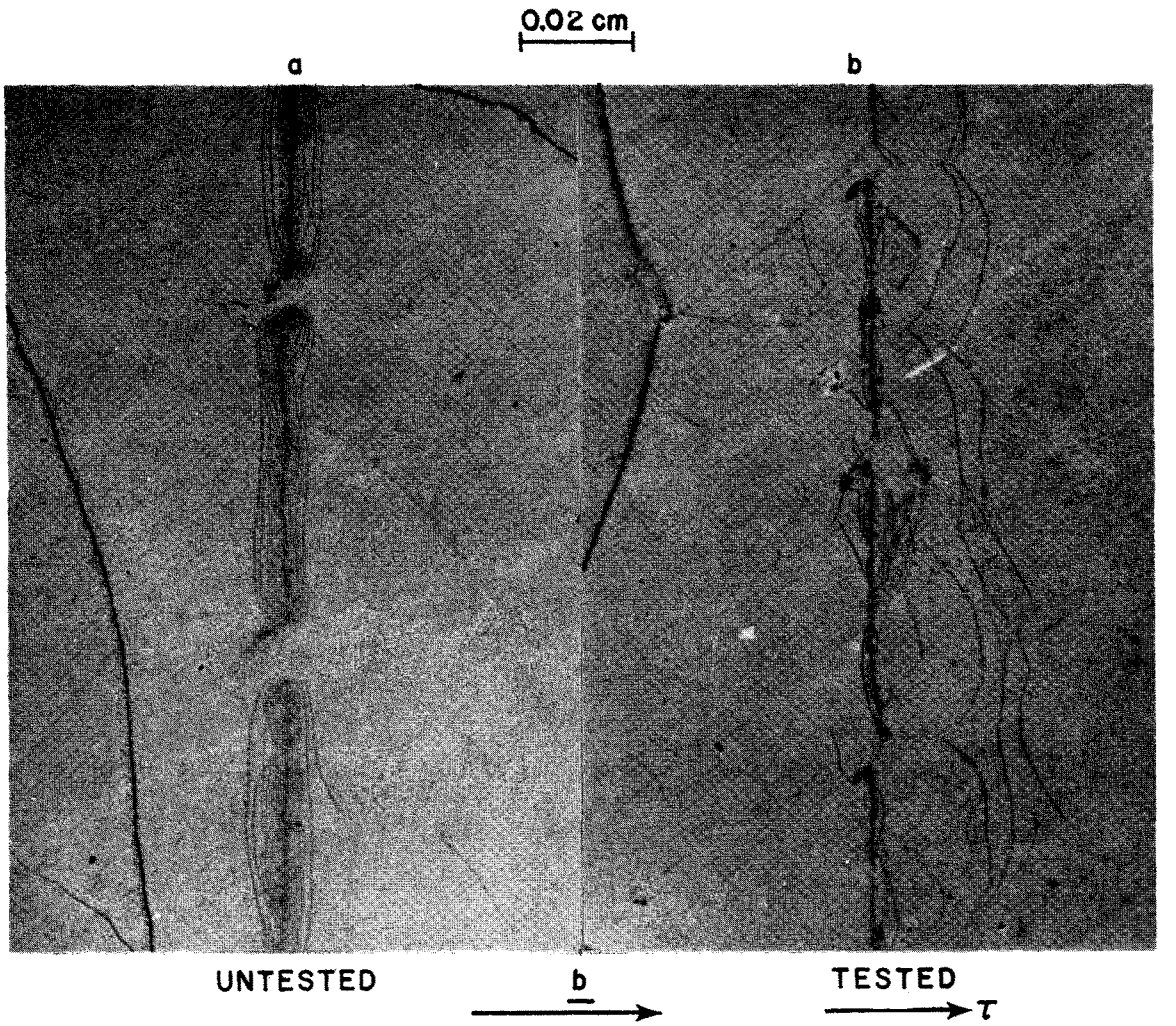

FIG. 2. Berg–Barrett photographs of dislocations around scratch segments on a tested and an untested specimen. (Two different specimens.)

rods were such that the load duration at the observation surface (interface between the specimen and the monel bar) ranged from 47–94 μsec.

EXPERIMENTAL RESULTS

Dislocation Displacement Measurements

Figure 2 shows Berg–Barrett photographs of the dislocation arrangement around three scratch segments before and after testing. The two photographs were not taken from the same specimen for reasons stated earlier in this paper.

The sign of the dislocation Burgers vectors around the scratch in Fig. 2(a) can be deduced from the following argument. The scratching process produces a shear stress in the specimen which pushes the material to either side of the scratch. Such a deformation process should produce edge dislocations whose extra half-plane of atoms extends to the free surface from the dislocation lines. If the dislocations are of this sign they should move in the direction of the shear stress applied to the surface. This is observed in Fig. 2(b). There were isolated instances of motion in the opposite direction indicating the generation of some dislocations of the opposite sign.

The maximum distance of dislocations from each scratch segment was measured on the Berg–Barrett photographs. The measurements were made at every scratch segment at which the displacements were measurable. Measurements were not made on scratch segments where the dislocation motion appeared to be impeded by subboundaries. The results of these measurements are shown in Fig. 3 plotted as a function of radial position on the specimen. Within experimental scatter, the distance of the dislocation farthest from the scratch after stress application is linearly proportional

to radial position, as indicated by the least-squares-fit line drawn in each plot.

The displacements plotted in Fig. 3 are the sum of the displacement due to scratching and the displacement due to loading. The displacement due to scratching, for any given test, was taken to be the intercept with the displacement axis of the line drawn to represent the data in Fig. 3. The values so determined are consistent with measurements made on the scratched but untested specimen shown in Fig. 2. These values of dislocation displacement due to scratching were subtracted from the measured total dislocation displacements to obtain the maximum displacement which occurred during the applied stress pulse. Dislocation velocities were computed from these latter displacement values.

Stress and Time Measurements

The stress-pulse magnitude and duration must be known in order to determine dislocation velocity as a function of applied shear stress from the dislocation displacement measurements. Figure 4 shows four records of the strain-gauge output for four different stress pulses. The top trace in each photograph shows the strain–time history in the Monel bar over a period of 2 msec, while the bottom trace shows the main pulse in the top trace on an expanded time scale. The top traces show that only one pulse of significant amplitude is applied to the specimen. The record in Fig. 4(a) shows the shape of a pulse which occurs when a titanium extender is glued directly to the Monel strain-gauge bar without a specimen in between. The salol glue layer was made very thin to minimize effects of the large compliance of the salol. The titanium extender was made 1.15 cm in diam so that its torsional acoustic

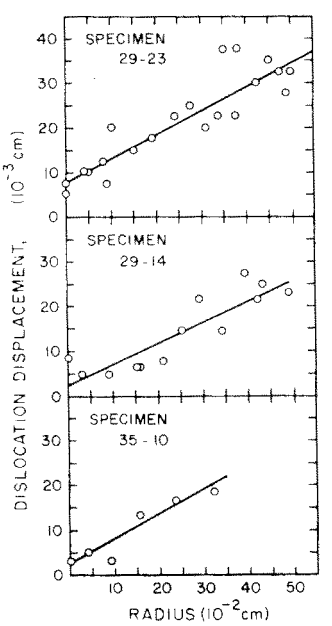

FIG. 3. Dislocation displacement plotted against radial position.

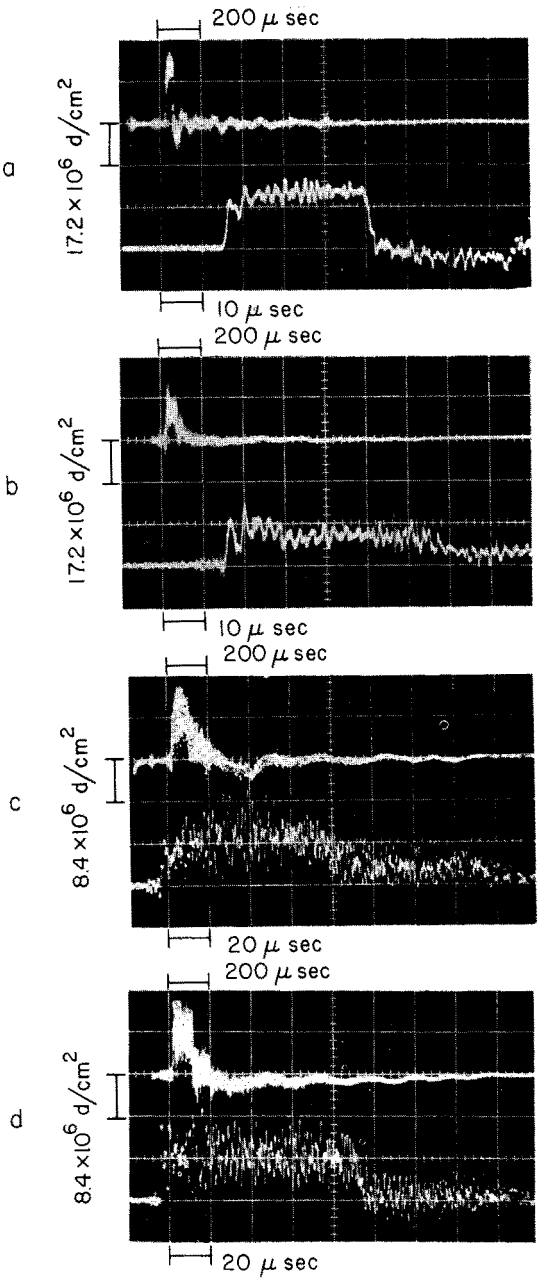

FIG. 4. Four strain records. (a) Record obtained with titanium extender glued directly to Monel strain gauge bars. (b), (c), and (d) Records from tests on specimens 29-23, 29-14, and 35-10, respectively.

impedance is the same as the 1.10-cm-diam zinc specimens. Therefore, the strain-gauge output in Fig. 4(a) is the same as for a zinc specimen behaving completely elastically fastened to the Monel rod with a thin glue layer. Referring to the bottom trace in Fig. 4(a), the stress rises within a few microseconds, reaches a plateau with some changes in level probably due to friction in the torsion machine, drops to zero, becomes slightly negative due to the acoustical mismatch between the

TABLE I. Values of τ_{eff} and t_0.

Specimen	τ_{eff} (10^6 dyn/cm^2) maximum	t_0 (μsec)
29–23	17.3	47
29–14	12.8	73
35–10	9.7	94

Monel and titanium, and finally returns to zero. Fig. 4(b) shows the strain-gauge record from the test on specimen 29–23 in which the applied torque was the same as in Fig. 4(a). The differences in shape between the pulses in Fig. 4(a) and 4(b) are due to the large compliance of the thick glue layer used in the test shown in Fig. 4(b) and plastic flow in the specimen. The compliance of the glue bond is probably the biggest effect. The cause of the high-frequency stress components in the records shown in Fig. 4(c) and (d) is not known. The amplitude of these components seems to be independent of the amplitude of the input torque.

The plastic strain in the specimen is small compared to the elastic strain as shown by the following argument. The maximum dislocation motion measured on specimen 29–23 was about 0.020 cm at stress of 11.3×10^6 dyn/cm^2. If all the basal dislocation length of 2×10^4 cm/cm^3 in the crystal moved that far the plastic strain would be 16×10^{-6}. The elastic strain at that stress was 29×10^{-6}. Since the dislocations in the bulk crystal are not all mobile nor are they all oriented such as to be moved by the maximum applied stress, the plastic strain must be far smaller than 16×10^{-6}. Therefore the stress distribution in the specimen must very nearly approximate the elastic distribution, namely the shear stress is linearly proportional to radial position. From Fig. 3 the dislocation displacements are also linear functions of radial position. Therefore, since the applied stress and the dislocation displacements are linear with radius, and since the time dependence of stress is independent of radius, dislocation velocity is a linear function of applied shear stress.

Since the stress pulses of Fig. 4 are not rectangular, an effective pulse duration and an effective stress were defined as follows. The dislocation displacements at any radial position are directly proportional to the time integral of the stress at that radius, where the integral is taken over the total duration t_1 of the stress pulse, i.e.,

$$D=\int_0^{t_1} v(t)\,dt=K\int_0^{t_1}\tau(t)\,dt=K\tau_{eff}t_0, \qquad (2)$$

where $v(t)$ is the instantaneous dislocation velocity, K is constant, $\tau(t)$ is the instantaneous stress, τ_{eff} is the effective stress for a square pulse of duration t_0, and t_0 is the effective pulse duration which is equal to the round-trip travel time of an elastic wave through the specimen and titanium extender.

The effective stress at the maximum radius was determined for each specimen by performing the time integral of stress on each stress record with a planimeter and dividing the integral by t_0. Values of τ_{eff} and t_0 are given in Table I.

Dislocation Velocities

Dislocation velocities were calculated by dividing the dislocation displacement due to the load pulse by the effective pulse duration t_0. The dislocation-velocity–stress data are plotted in Fig. 5. The velocities were determined as described above and the associated stresses are the effective stresses also determined as described above, assuming that the shear stress is a linear function of radius. Velocities were calculated only for those values of total displacement $\geq2\times10^{-3}$ cm since the uncertainty in the displacement due to scratching makes the relative error in total displacement unreasonably large for smaller values. The data in Fig. 5 are fitted with the straight line

$$v=3.4\times10^{-5}\tau, \qquad (3)$$

where v is in cm/sec and τ is in dyn/cm^2. The scatter in the data shown in Fig. 5 is greater than can be accounted for by the uncertainties in the measurements of stress ($\pm10\%$), dislocation displacement ($\pm2\times10^{-3}$ cm), and time ($\pm5\%$). A possible source of the scatter in the data is discussed later in this paper.

DISCUSSION

Effect of Line Tension

The line tension of a curved dislocation could influence the results of this study by modifying the net

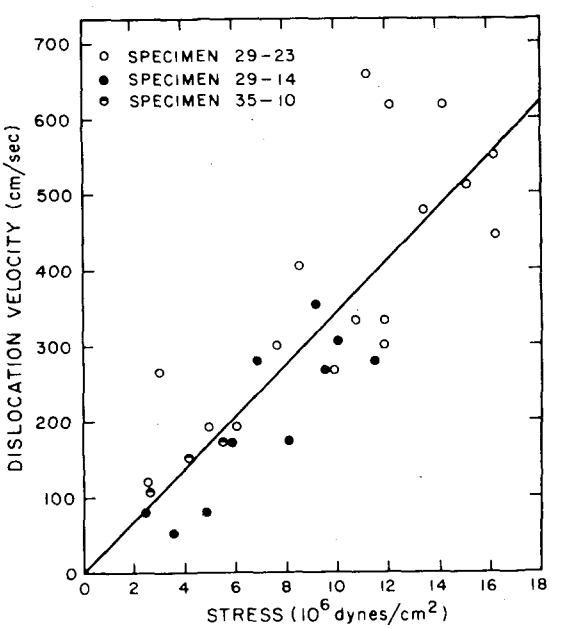

FIG. 5. Plot of measured dislocation velocity as a function of applied, resolved shear stress.

force on the dislocation. A typical radius of curvature of the dislocations on a tested specimen is 0.018 cm. The stress required to maintain this radius is about 0.3×10^6 dyn/cm^2, a small stress compared to the applied stresses in this work. The radii of curvature of dislocations around a scratch on an untested specimen are larger than 0.018 cm except near the ends of the scratch segments, as can be seen in Fig. 2(a). Therefore, the effect of dislocation line-tension is negligible compared to that of the applied stresses in this work.

Effect of Dislocation Interactions

The stress fields of nearby dislocations can materially affect the stress acting on a dislocation. The dislocations around the scratches were spaced about 6×10^{-4} cm apart before testing. Non-negligible interaction forces between the dislocations can occur at this spacing. However, after the tests the dislocations are much more widely spaced, so that interaction forces are then definitely negligible. Therefore, it is concluded that the basal dislocations are spaced widely enough during most of their motion that interaction forces between them can be neglected.

Typical forest dislocation densities are 10^3–10^4 cm^{-2} in these crystals. Thus the moving basal dislocations intersected forest dislocations every 0.01–0.04 cm. Since forest dislocations are known to interact strongly with basal dislocations,[10] such interactions could be responsible for much of the scatter in the data.

Effect of Pinning due to Point Defects

The dislocation velocity at a given applied shear stress may be influenced by the presence of point defects in the dislocation core. The pinning of dislocations that occurs when specimens are aged before testing is probably due to the diffusion of point defects to the dislocations from the specimen surface. The effect of drag due to these defects on the data presented in this paper cannot be assessed. Every attempt was made to minimize the aging time before testing to minimize the number of these defects.

Comparison with Previous Work

Adams[8] measured the rate of growth of basal slip bands in zinc. He employed compression-stress pulses and used an etch to reveal the dislocations in the slip bands formed by the stress pulses. The dislocation velocities observed by Adams agree in magnitude with the velocities observed in the present work at comparable stress levels. However, scatter and the relatively small velocity range covered in Adams' data make comparison difficult.

Mechanisms for Limiting Dislocation Velocities

A number of theories predict dislocation mobility by assuming that the dislocations move in jumps from one obstacle to the next, and that the combined effect of thermal activation and the applied shear stress are required for the dislocation to overcome the obstacle. Various kinds of obstacles have been treated, including point defects[15,16] and forest dislocations.[17] However, the observed linear dependence of dislocation velocity on stress is not predicted by any of these thermally activated processes.

Another theory considers dislocation velocities to be limited by the interaction of the moving dislocation strain field with vibrations of the crystal lattice. The theory has been approached in various ways by Leibfried,[18] Eshelby,[19] Mason,[20] and has recently been unified and extended by Lothe.[21] Four different sources of dislocation drag have been treated: the thermoelastic effect, the core anharmonicity effect, the phonon-viscosity effect, and the phonon-scattering effect. According to Lothe, the thermoelastic effect is negligible in metals while the other three effects give rise to drag stresses of approximately the same magnitude. The total drag stress τ_D on a moving dislocation due to these three effects is

$$\tau_D\approx(3/10)\,(\epsilon/c_s)\,v. \tag{4}$$

ϵ is the thermal energy density $(3kT/V)$; k is Boltzmann's constant; V is the volume per atom $=14.7\times10^{-24}$ cm^3 in zinc. c_s is the shear-wave speed $=2.3\times10^5$ cm/sec. This theory is attractive because it not only predicts the observed linear dislocation-velocity–stress function but also predicts the correct order of magnitude of the constant of proportionality. Eq. (4) predicts

$$v\approx9\times10^{-5}\tau, \tag{5}$$

at room temperature with c_s taken as 2.3×10^5 cm/sec. This is to be compared to Eq. (3),

$$v=3.4\times10^{-5}\tau, \tag{3}$$

the experimentally determined relation. Considering that Eq. (4) yields only an order of magnitude estimate of the proportionality constant, the agreement between this theory and the present experimental results is very good.

Those theories which depend upon thermal activation for dislocations to overcome obstacles predict that dislocation velocities increase with increasing temperature. However, the phonon-drag theory predicts that dislocation velocities decrease with increasing temperature. The results of tests at different temperatures would help greatly in establishing the correct mechanism.

---

[15] J. J. Gilman, J. Appl. Phys. **36,** 3195 (1965).
[16] R. L. Fleischer, J. Appl. Phys. **33,** 3504 (1962).
[17] A. Seeger, S. Mader, and H. Kronmüller, *Electron Microscopy and Strength of Crystals* (Interscience Publishers, Inc., New York, 1963), p. 665.
[18] G. Leibfried, Z. Physik **127,** 344 (1950).
[19] J. D. Eshelby, Proc. Roy. Soc. (London) **A197,** 396 (1949).
[20] W. P. Mason, J. Acoust. Soc. Am. **32,** 458 (1960).
[21] J. Lothe, J. Appl. Phys. **33,** 2116 (1962).

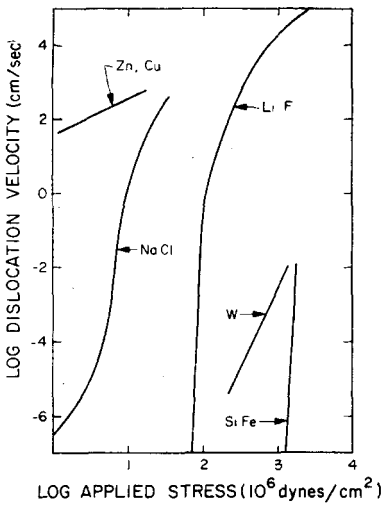

FIG. 6. Comparison of the mobility of dislocations in various materials at room temperature. Mobility data obtained from: LiF (Ref. 1), Si-Fe (Ref. 2), NaCl (Ref. 3), W (Ref. 4), Zn (work reported here), Cu (Ref. 9).

Comparison of Dislocation Mobilities in Zinc with Mobilities in Other Materials

The stress dependence of dislocation mobility in zinc differs markedly from all materials on which mobility measurements have been made with the exception of copper. This fact is illustrated in Fig. 6. Greenman[9] found that dislocations in copper obey the relation

$$v = 3.6 \times 10^{-5} \tau. \quad (6)$$

The phonon-drag theory predicts the mobility of dislocations in copper to be

$$v = 6.6 \times 10^{-5} \tau. \quad (7)$$

Hence, the phonon-drag theory predicts velocities that are approximately a factor of three too high for zinc and a factor of two too high for copper at room temperature. Suzuki *et al.*[22] have indirectly measured the damping stress on moving dislocations in copper by internal friction techniques. These investigators found that the damping stress on dislocations in copper does increase with increasing temperature, although not in the exact manner predicted by Eq. (4). It would be very useful and interesting to compare the results of the present investigation with results from internal friction measurements. However, suitable results from internal friction measurements on zinc are not presently available.

SUMMARY AND CONCLUSIONS

Basal dislocations of predominantly edge character were produced within a depth of about 5 μ below the basal plane observation surface of 99.999% pure zinc crystals by controlled scratching of the surface. Movement of these dislocations on their glide planes was produced by resolved shear stresses ranging from 0 to 17.2×10^6 dyn/cm^2 applied to the crystal surface for load durations ranging from 47–94 μsec. The distance through which the dislocations moved was determined from Berg–Barrett x-ray micrographs.

The dislocation velocities determined from the dislocation movement and the duration of stress ranged from 40–700 cm/sec and were linearly proportional to the stress. The experimental value of the ratio of dislocation velocity to applied resolved shear stress (3.4×10^{-5} cm^3 dyn^{-1} sec^{-1}) is in agreement, within experimental and theoretical uncertainties, with the theoretical value of 9×10^5 dyn·sec/cm^3 derived from the concept of the interaction between dislocations and the thermal vibrations of the crystal lattice (phonon-drag effect).

[22] T. Suzuki, A. Ikushima, and M. Aoki, Acta Met. **12**, 1231 (1964).